Geophysical Prospecting, 2009, **57**, 343–353 doi: 10.1111/j.1365-2478.2008.00740.x

Ground-roll attenuation using a 2D time-derivative filter

Paulo E. M. Melo, Milton J. Porsani* and Michelângelo G. Silva

Centro de Pesquisa em Geofísica e Geologia, Instituto de Geociências, Universidade Federal da Bahia, Campus Universitário da Federação, Salvador, Bahia, Brazil

Received May 2007, revision accepted July 2008

ABSTRACT

We present a new filtering method for the attenuation of ground-roll. The method is based on the application of a bi-dimensional filter for obtaining the time-derivative of the seismograms. Before convolving the filter with the input data matrix, the normal moveout correction is applied to the seismograms with the purpose of flattening the reflections. The method can locally attenuate the amplitude of data of low frequency (in the ground-roll and stretch normal moveout region) and enhance flat events (reflections). The filtered seismograms can reveal horizontal or sub-horizontal reflections while vertical or sub-vertical events, associated with ground-roll, are attenuated. A regular set of samples around each neighbourhood data sample of the seismogram is used to estimate the time-derivative. A numerical approximation of the derivative is computed by taking the difference between the interpolated values calculated in both the positive and the negative neighbourhood of the desired position. The coefficients of the 2D time-derivative filter are obtained by taking the difference between two filters that interpolate at positive and negative times. Numerical results that use real seismic data show that the proposed method is effective and can reveal reflections masked by the ground-roll. Another benefit of the method is that the stretch mute, normally applied after the normal moveout correction, is unnecessary. The new filtering approach provides results of outstanding quality when compared to results obtained from the conventional FK filtering method.

INTRODUCTION

In seismic exploration, the noise present in seismograms with trace-to-trace regularity is classified as coherent noise. Among these types of noise, ground-roll, present in land and ocean bottom seismic surveys, is responsible for a significant reduction in the signal-to-noise ratio. The ground-roll is associated with Rayleigh-type surface waves that occur in the zone of low velocity near the surface (Yilmaz 1987). It occurs in land and ocean bottom seismic data dominating some portions of the seismograms, interfering and, therefore masking the seismic reflections of interest. The attenuation or removal of this kind of noise represents a serious obstacle to the processing of seismic data. The main characteristics of this noise are its high amplitude, low velocity, dispersion and the concentration of energy in the low frequencies.

Several papers have been published in geophysics literature investigating methods for the attenuation of the ground-roll. Some of them show that the ground-roll can be attenuated during the acquisition, through special source and receiver arrays (Anstey 1986; Pritchett 1991). Such a strategy may have logistical limitations or be unusable on data already acquired (Harlan, Claerbout and Rocca 1984; Shieh and Herrmann 1990). Other authors have tried new approaches based on filtering methods applied in the frequency, Radon or wavelet domains, or have applied numerical transformations such as Karhunen-Loeve and SVD, or have used polarization filters and multi-component data (Claerbout 1983; Saatçilar 1988; Song and Stewart 1993; Liu 1999; Henley 2003; Kendall, Jin and Ronen 2005; Yarham, Boeniger and Herrmann 2006). One of

*E-mail: porsani@cpgg.ufba.br

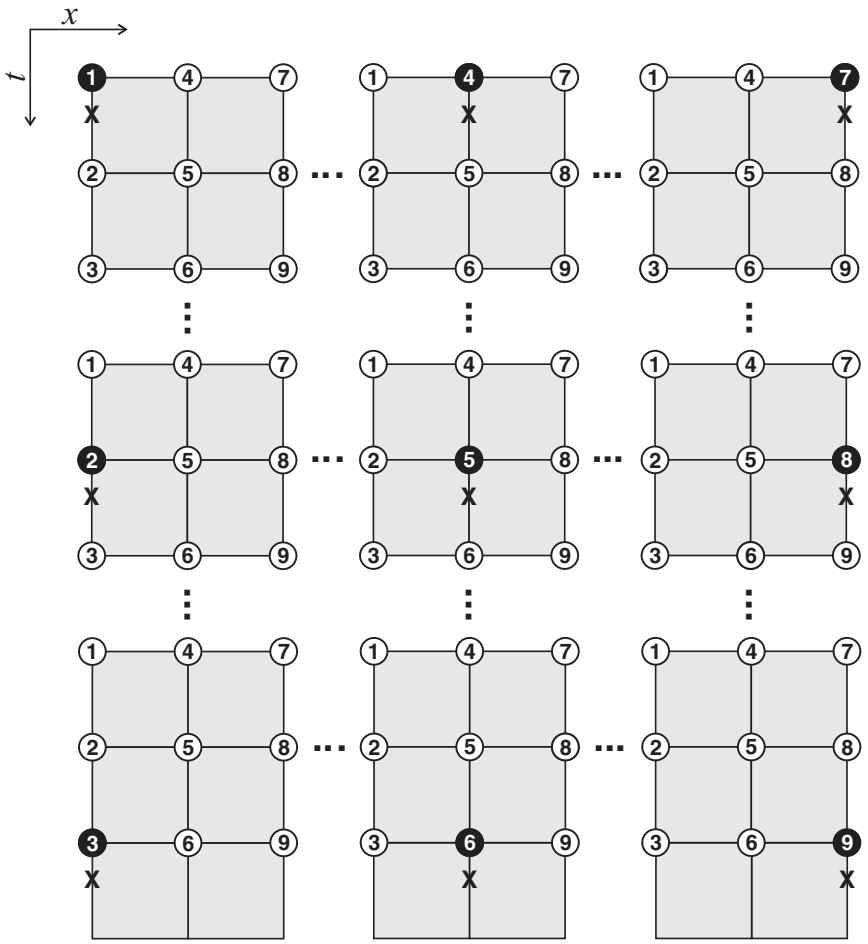

Figure 1 Schematic representation of the geometry of a (3 × 3) interpolation operator $\mathbf{O}_j^+$. Its central position is indicated by the black circle, which also identifies the operator. The cross symbol in boldface indicates the desired position for the output, shifted for positive times, where the distances to the data are used for calculation of the weights w_i^+.

the simplest filtering approaches used in the ground-roll attenuation problem, is FK filtering, based on the 2D Fourier transform (Embree, Burg and Backus 1963; Wiggins 1966). The ground-roll, represented by linear events with low velocities, is mapped as lines in the FK domain and can consequently be filtered by using a 2D band-pass filter.

Although the FK method is effective in the removal of linear events, it also attenuates any primary reflected signals present in the frequency band and dip range of the ground-roll.

This paper presents a new filtering method for ground-roll attenuation using a 2D time-derivative filter. Before convolving the filter with the data matrix, the normal moveout (NMO) correction is applied to the seismograms with the purpose of flattening the reflections. We illustrate the method by using land seismic data from the Tacutu basin, located in the northeast of Brazil. The seismic data was acquired by PETROBRAS in 1981 (Eiras and Kinoshita 1990).

This paper is organized in the following way: First, we present the method that is used to generate the 2D derivative filter. Next, we present numerical results using real seismic data. Finally, we present the conclusions.

A 2D TIME DERIVATIVE FILTER

Let $f(x, t)$ represent the wave field recorded in the seismogram. A numerical approximation of the first time-derivative of the function $f(x, t)$ may be calculated with the expression,

$$\frac{\partial f(x,t)}{\partial t} \approx \frac{f(x,t+\delta_t) - f(x,t-\delta_t)}{2\delta_t}, \tag{1}$$

where $\delta_t > 0$ represents a perturbation in the time variable.

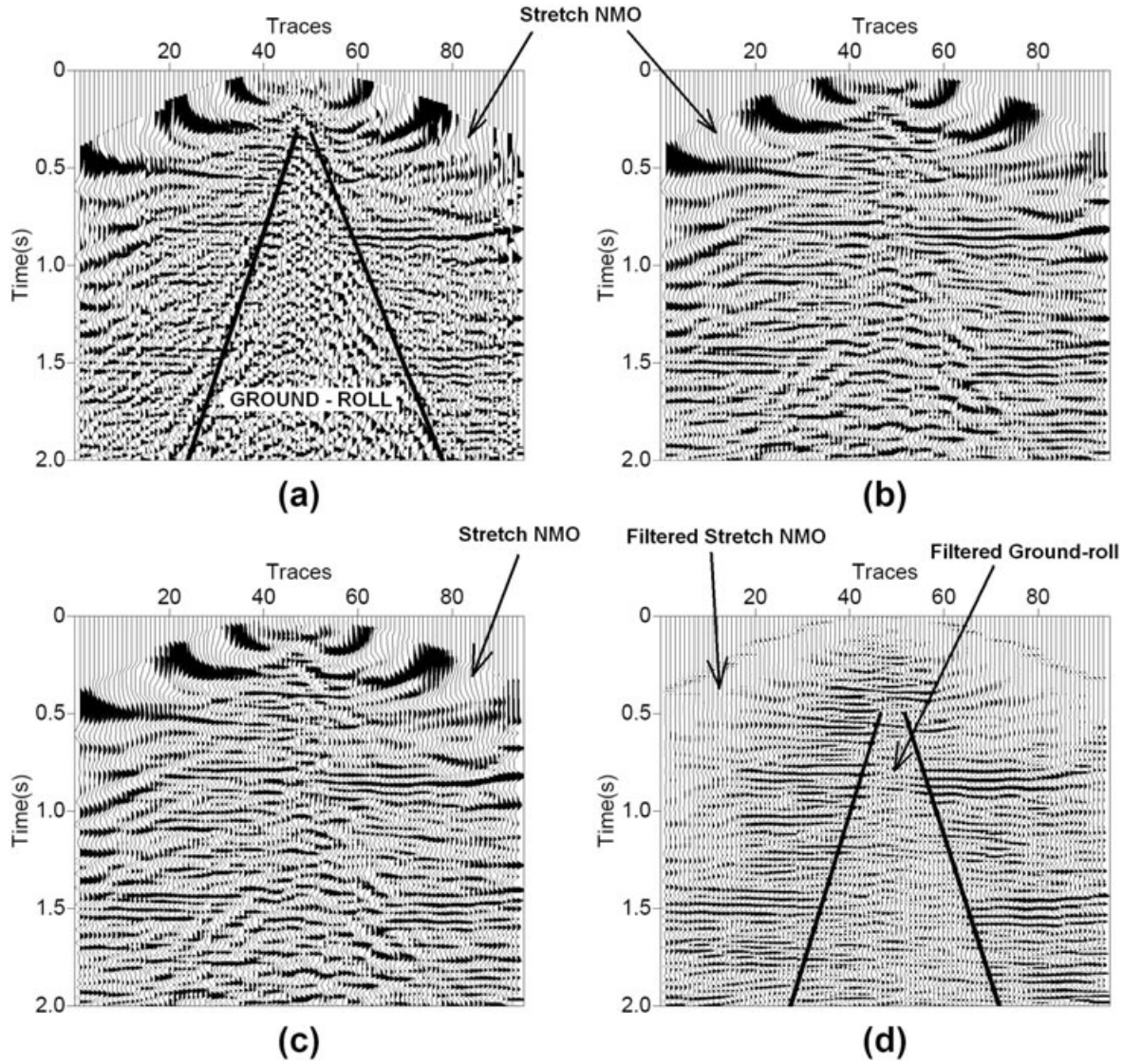

Figure 2 Original shot-gather after NMO correction in (a). Forward interpolation using $\mathbf{O}_j^+$ in (b). Backward interpolation using $\mathbf{O}_j^-$ in (c). Difference between results in (b) and (c) is shown in (d).

$\mathbf{D}_t^1$

- 0.090045	- 0.040270	- 0.021839
0.129087	0.015564	- 0.007858
0.013811	0.005153	- 0.003603

$\mathbf{D}_t^4$

- 0.037721	- 0.084347	- 0.037721
0.012926	0.114429	0.012926
0.003934	0.011640	0.003934

$\mathbf{D}_t^7$

- 0.021839	- 0.040270	- 0.090045
- 0.007858	0.015564	0.129087
- 0.003603	0.005153	0.013811

$\mathbf{D}_t^2$

- 0.159102	- 0.040538	- 0.010151
0.000000	0.000000	0.000000
0.159102	0.040538	0.010151

$\mathbf{D}_t^5$

- 0.036320	- 0.142545	- 0.036320
0.000000	0.000000	0.000000
0.036320	0.142545	0.036320

$\mathbf{D}_t^8$

- 0.010151	- 0.040538	- 0.159102
0.000000	0.000000	0.000000
0.010151	0.040538	0.159102

$\mathbf{D}_t^3$

- 0.013811	- 0.005153	0.003603
- 0.129087	- 0.015564	0.007858
0.090045	0.040270	0.021839

$\mathbf{D}_t^6$

- 0.003934	- 0.011640	- 0.003934
- 0.012926	- 0.114429	- 0.012926
0.037721	0.084347	0.037721

$\mathbf{D}_t^9$

0.003603	- 0.005153	- 0.013811
0.007858	- 0.015564	- 0.129087
0.021839	0.040270	0.090045

Figure 3 Coefficients of the 2D filters used in obtaining the first time-derivative of the seismograms.

As in the Taylor expansion method, the surrounding samples to a given position $\mathbf{r} = (x, t)$ may be used to estimate the partial derivatives.

Let $I(\mathbf{r}^+)$ and $I(\mathbf{r}^-)$ represent approximations of the function $f(x, t)$ in the positive $\mathbf{r}^+ = (x, t + \delta_t)$, and negative $\mathbf{r}^- = (x, t - \delta_t)$ neighbourhood time position, calculated by using a linear interpolation method:

$$f(\mathbf{r}^+) \approx \sum_{i=1}^{N} w_i^+ A_i = I(\mathbf{r}^+) \tag{2}$$

$$f(\mathbf{r}^-) \approx \sum_{i=1}^{N} w_i^- A_i = I(\mathbf{r}^-) \tag{3}$$

where:

N is the number of data samples used in the linear interpolation;

A_i represents the amplitude of the input data matrix at position $\mathbf{r}_i$, taken in the neighbourhood of the desired position $\mathbf{r}$ and

$\{w_i^+, w_i^-\}$ represents the coefficients used in the interpolation at positions $\mathbf{r}^+$ and $\mathbf{r}^-$ respectively.

Using equations (2) and (3) in equation (1) we obtain:

$$\frac{\partial f(x,t)}{\partial t} \approx \frac{I(\mathbf{r}^+) - I(\mathbf{r}^-)}{2\delta_t} = \sum_{i=1}^{N} \frac{(w_i^+ - w_i^-)}{2\delta_t} A_i \quad . \tag{4}$$

Equation (4) gives a numerical approximation of the time-derivative from the difference between the interpolated values taken at two positions close to the desired position. In order to evaluate directly the time-derivative by using only one 2D filter, we combine the coefficients of the two interpolation operators into one:

$$\mathbf{D}_t = \mathbf{O}^+ - \mathbf{O}^- = \left\{ \frac{(w_i^+ - w_i^-)}{2\delta_t}, i = 1, \ldots, N \right\} \quad . \tag{5}$$

The computational implementation is simplified by considering the data matrix (seismograms) as corresponding to a regular grid. In this case we may design a 2D filter and the derivative may be obtained by convolving it with the data matrix. The first derivative with respect to time is given by:

$$\mathbf{A}'_t = \mathbf{A} * \mathbf{D}_t \, , \tag{6}$$

where $*$ represents the convolution, $\mathbf{D}_t$ represents the 2D filter to evaluate the first derivative and $\mathbf{A}$ represents the $(N_t \times N_x)$ input data matrix associated with the seismograms. The first derivative filter can be applied in cascade to generate higher order derivatives.

The derivative with respect to the spatial variable x, if desired, may be obtained in a similar way. In the case of a regular grid, with equal x and t sampling intervals, we can use the transpose of the operator, or the transpose of the data matrix to obtain the derivative with respect to the x variable:

$$\mathbf{A}'_x = \mathbf{D}_t^T * \mathbf{A} = \mathbf{D}_t * \mathbf{A}^T \, . \tag{7}$$

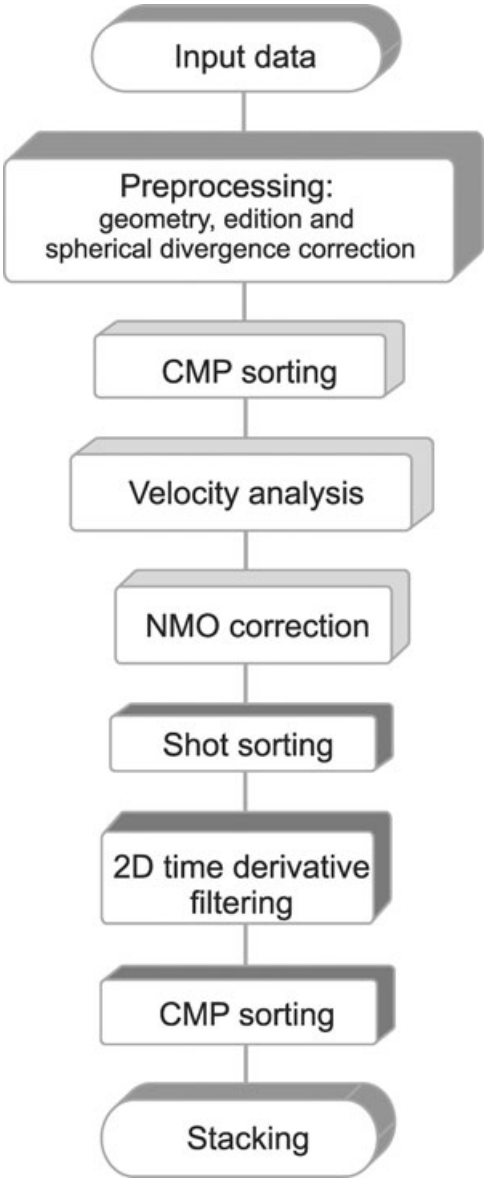

Figure 4 Flowchart of the seismic processing used in obtaining the stacked section.

Obtaining the interpolation weights

A very simple approach to compute the weights w_i required in equations (2) and (3) is given by the Shepard method (Shepard 1968). By using this method we can compute the interpolation

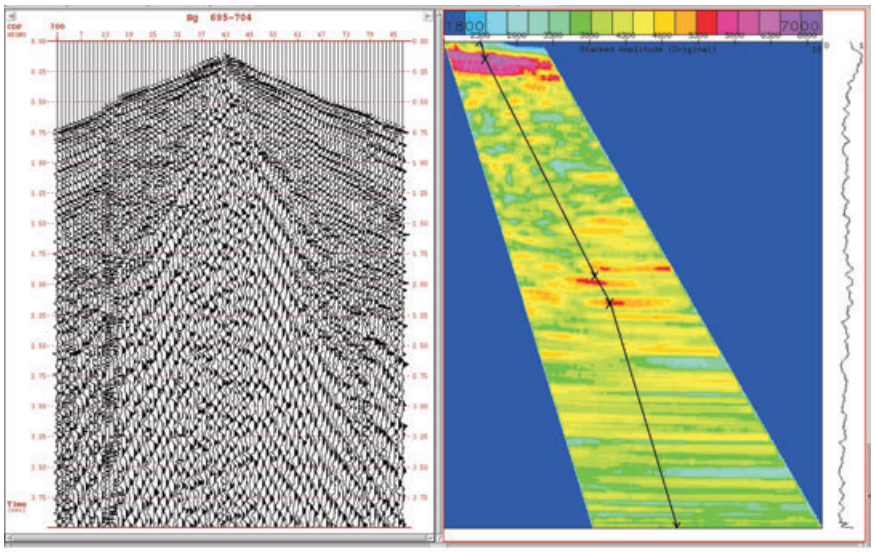

Figure 5. Super-gather formed by 10 CMPs in (a) and its corresponding velocity analysis in (b).

weights based on the inverse of the distance:

$$w_j = \frac{\frac{1}{d_j}}{\sum_{i=1}^{N} \frac{1}{d_i}}. \tag{8}$$

where $d_i = |\mathbf{r} - \mathbf{r}_i|$ represents the distance between the position $\mathbf{r}$ of the desired output where we want to interpolate and the data position $\mathbf{r}_i$. It can be shown that the Shepard method reproduces the data values at its original positions i.e., $I(\mathbf{r}_i) = A_i$.

In the case of a regular grid, the coefficients w_i of an $N \times N$ interpolation operator need to be generated only once and applied to all data matrix by means of convolution, making the interpolation method simple and computationally efficient.

Equation (8) may be used in the computation of the weights w_i^+ and w_i^- required in equation (5). We point out that the proposed method may be used to generate 2D operators to evaluate the derivative in any direction.

Figure 1 shows the geometry used in designing the 3×3 interpolation operators $\mathbf{O}_j^+$ for the positive neighbourhood of time. The number represented inside the black circle identifies the operator and indicates its central position. The cross, in boldface, indicates the output position to obtain the interpolated value. As indicated in the figure, the operators $\mathbf{O}_1^+, \mathbf{O}_3^+, \mathbf{O}_7^+$ and $\mathbf{O}_9^+$ are used only in the vertexes of the input matrix; the operators $\mathbf{O}_2^+, \mathbf{O}_4^+, \mathbf{O}_6^+$ and $\mathbf{O}_8^+$ are used to interpolate along the sides of the input matrix. The operator $\mathbf{O}_5^+$ is used for interpolating all remaining points and works in the interval $\{2 \le x_i \le N_x - 1\}$ and $\{2 \le t_i \le N_t - 1\}$.

Figure 2 shows the results obtained by applying the operators $\mathbf{O}_j^+$ and $\mathbf{O}_j^-$ in a shot-gather corrected for NMO (Fig. 2a). The interpolated forward ($\mathbf{O}_j^+$) and backward ($\mathbf{O}_j^-$) results are shown in Figs 2(b) and 2(c), respectively. Figure 2(d) shows the difference between results in Figs 2(b) and 2(c). In the region of the stretch (0.0–0.6s), the low frequency of the input data implies approximately equal results for the forward and backward interpolation and, consequently, the stretch is considerably removed as shown in Fig. 2(d).

As presented in Fig. 2 the method can locally attenuate the amplitude of low frequency data (in the NMO stretch region) and may emphasize the flat events (reflections).

Figure 3 contains the coefficients of the derivative filters calculated using equation (5). The time and the spatial sampling intervals of the data matrix were considered equal ($\Delta x = \Delta t = 1$). The perturbation in the time variable, δ_t, used in the evaluation of the numeric derivative was defined as half of the sampling interval, $\delta_t = \Delta t/2$. One may notice that the filters $\mathbf{D}_t^2, \mathbf{D}_t^5$ and $\mathbf{D}_t^8$ are anti-symmetrical, with respect to the time variable. The 2D derivative operator is applied by means of the convolution. Its output may also be considered to be the result of a weighted mixing process applied to the first time-derivative of the traces, using a sliding spatial window, along the offset direction.

NUMERICAL EXAMPLES

In this section we test the proposed method on a land seismic line. A shot-gather is used for comparing the results obtained

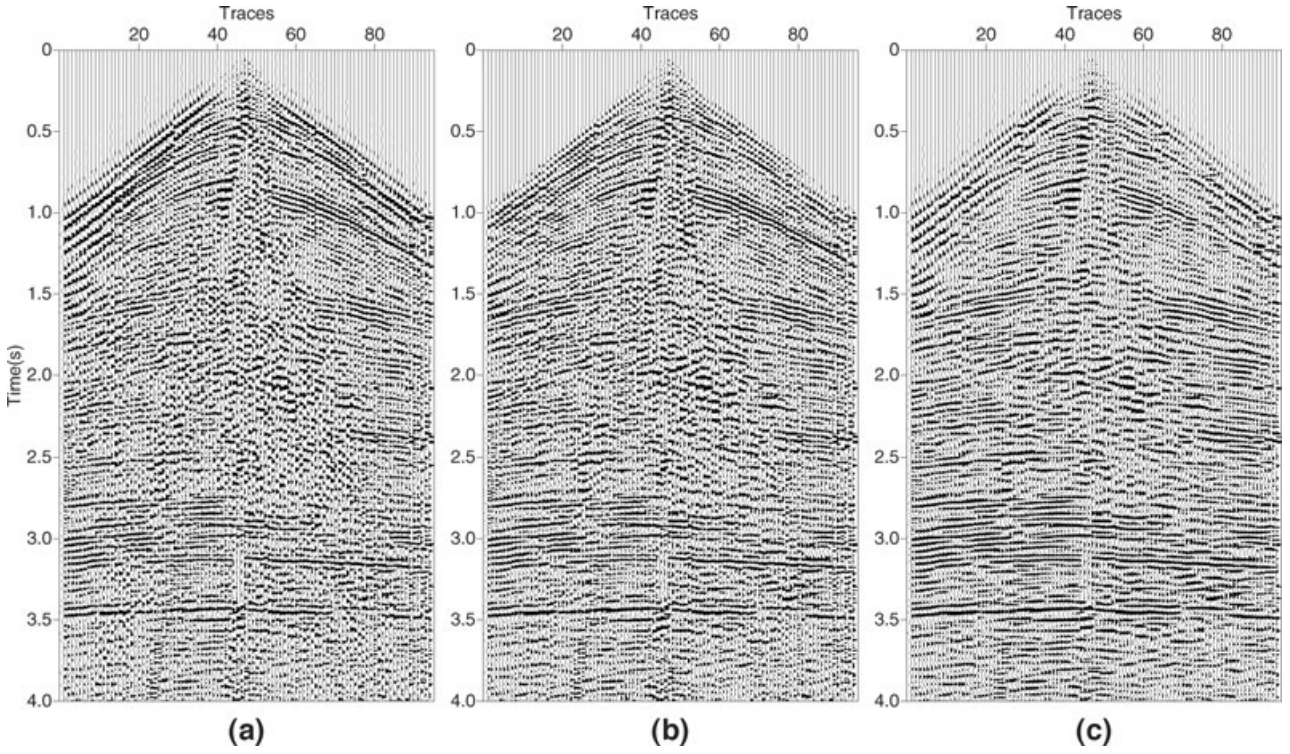

Figure 6 Filtered shot-gather. The output of the low-cut filter is shown in (a). The FK result is shown in (b). The result of mixing three adjacent traces of (a) is shown in (c).

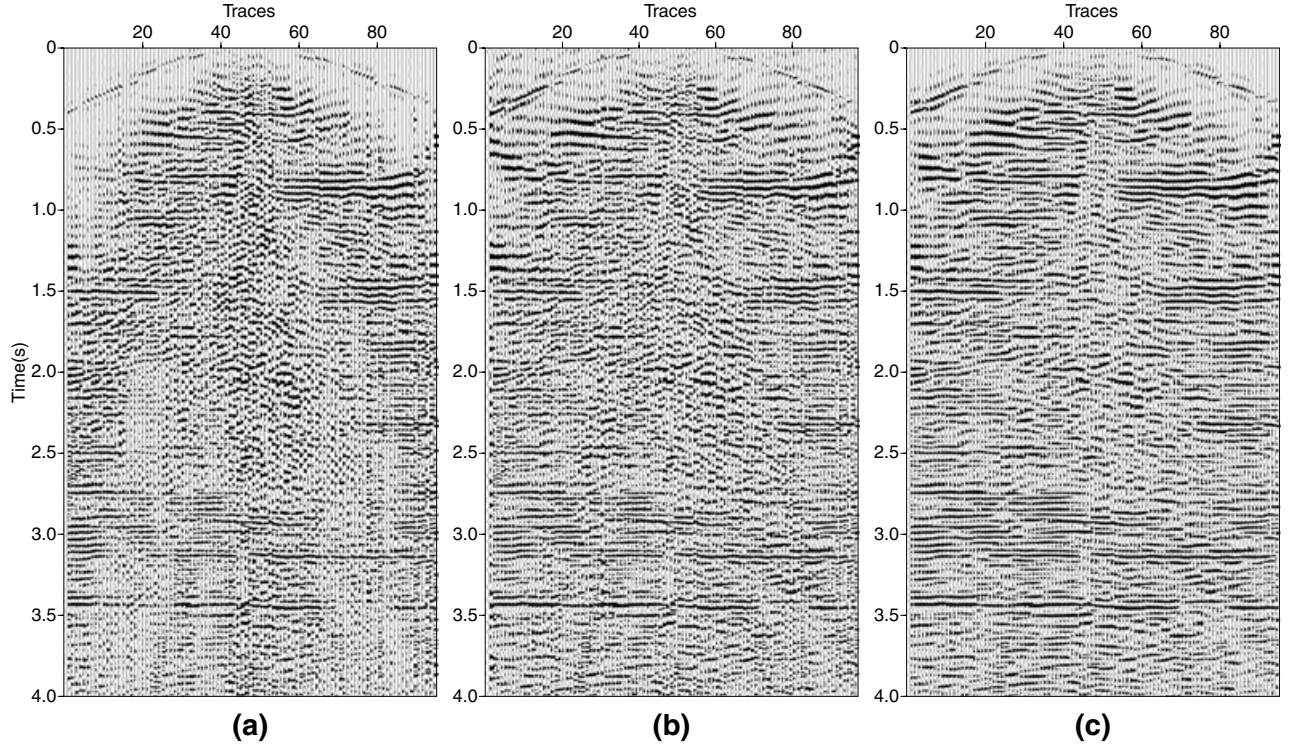

Figure 7 Filtered shot-gather after NMO correction. The output of the low-cut filter is shown in (a). The FK result is shown in (b). The result of mixing three adjacent traces of (a) is shown in (c).

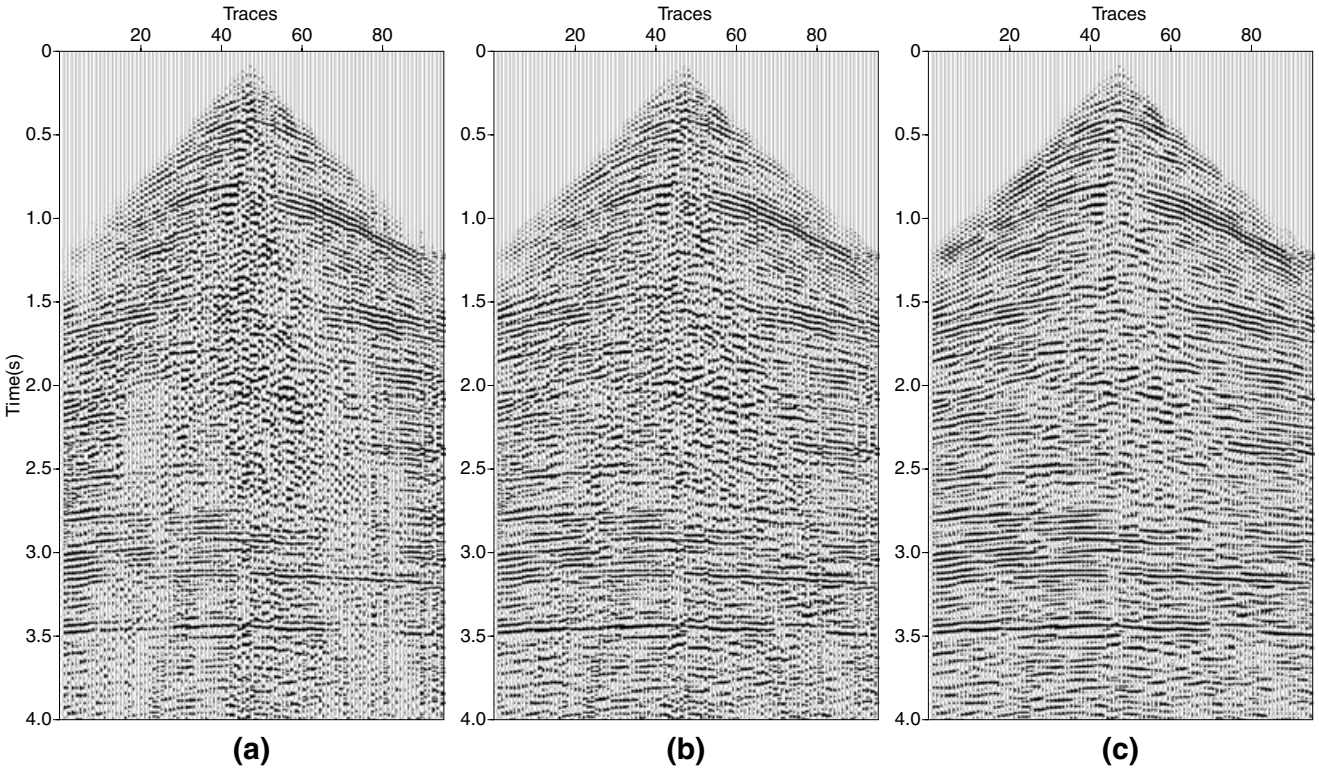

Figure 8 Reverse NMO correction of shot-gathers presented in Fig. 7. The output of the low-cut filter is shown in (a). The FK result is shown in (b). The result of mixing three adjacent traces of (a) is shown in (c).

using the following methods: low-cut, FK, low-cut plus mix and the proposed 2D time-derivative approach.

The seismic line used in the numerical examples contains 179 shots recorded at 4 ms sampling interval. The acquisition parameters were: split-spread geometry, offsets of 2500-150-0-150-2500 m, 12-fold common-midpoint (CMP), 96 channels/shot, distance between geophones 50 m and distance between shot points 200 m. The main problems with such seismic data are its low signal-to-noise ratio, due to the presence of the ground-roll and the low CMP coverage (fold of 1200%).

Before filtering the ground-roll we pre-processed the data using the following sequence: geometry, noise edit, mute, conventional CMP velocity analysis and NMO correction. Figure 4 presents the flowchart used in the processing of the RL-5090 seismic line.

Figure 5 shows the velocity analysis of a super-gather formed by 10 CMPs. The presence of the ground-roll seriously masks the reflections thus damaging the velocity determination.

A shot-gather was used in the testing of the following conventional filtering approaches: low-cut, FK and low-cut plus mix. Figure 6(a) shows the result of the low-cut filter (10–15) Hz. The result of FK filtering is presented in Fig. 6(b). The reject polygon is located between 10 and 20 Hz. Figure 6(c) shows the result obtained by mixing three adjacent traces of Fig. 6(a).

As illustrated in Fig. 5, an initial velocity analysis was performed and applied to all CMPs. Due to the low CMP coverage of the survey the seismic traces were reorganized in the common-shot gather after the NMO correction. In this domain, the reflections are approximately flattened, as shown in Fig. 7. Figures 7(a), 7(b) and 7(c) show the output of the low-cut, FK and the trace mix approach applied to the shot-gather with NMO correction. We observe that the stretched data in the interval 0.0–0.6s was considerably attenuated.

By applying the reverse NMO to the data shown in Fig. 7 we obtain the filtered shot-gathers shown in Fig. 8. These results should be compared with Fig. 6. The improvement in the signal-to-noise ratio, obtained specially in the region of the shallow reflections, between 0.0–1.3 s may be observed in Figs. 8(a), 8(b) and 8(c). All three filtering approaches that were used provide better results when applied after the NMO correction. They take advantage of the horizontal coherence of the reflections generated by the NMO correction. As the

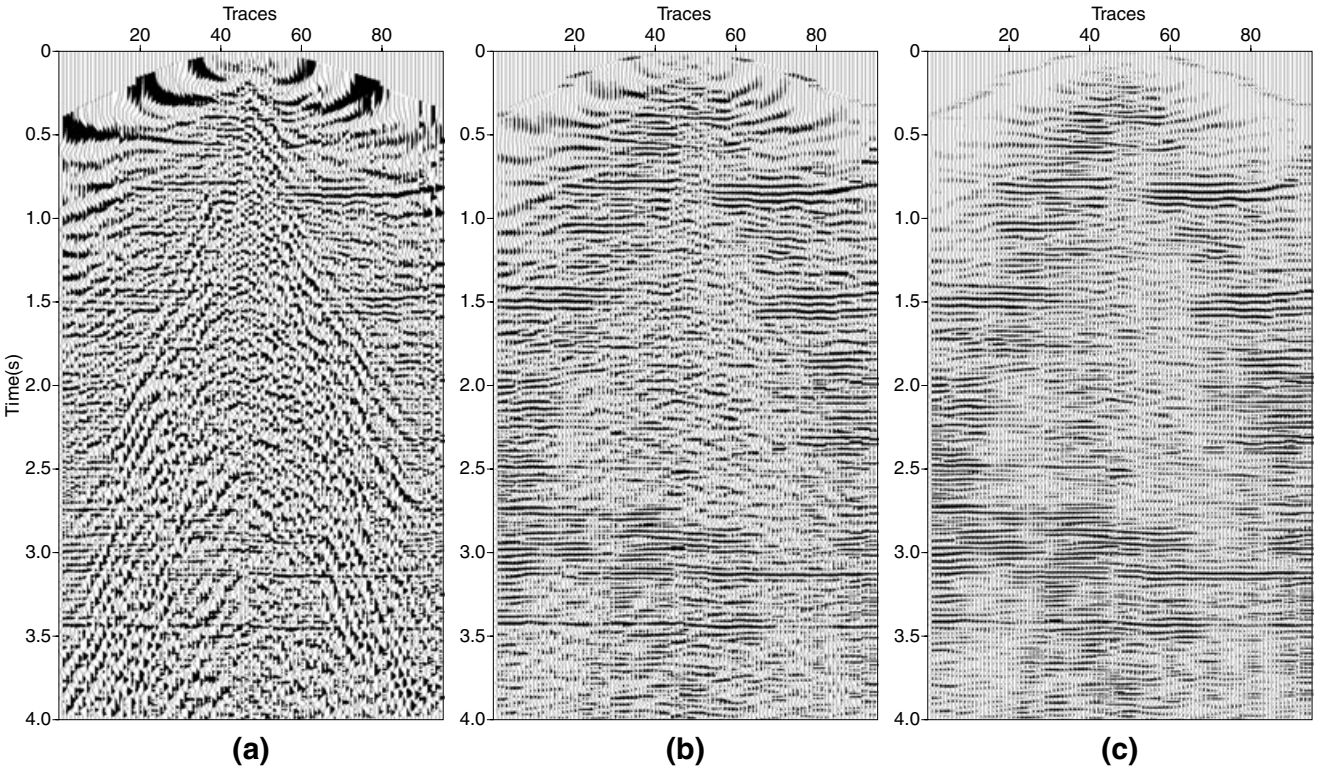

Figure 9 Results of the first and second 2D time-derivative applied to a shot-gather after NMO correction. The original shot-gather after the NMO correction is shown in (a). The first and second 2D time-derivatives are shown in (b) and (c), respectively.

ground-roll is not flattened by the NMO correction, it is partially attenuated during the 2D filtering process, as indicated by the low-cut plus mix results, shown in Fig. 8(c).

In the next examples we illustrate the application of the 2D time-derivative approach to attenuate the ground-roll and at the same time to reinforce the reflections. The filtering was applied to shot-gathers after NMO correction. We used the initial velocity obtained from the velocity analysis of super-gathers formed by 10 CMPs, as presented in Fig. 5.

Figure 9 shows the results of the 2D first and second time-derivative of the shot-gather used in the numerical experiments. The input data matrix, formed by the shot-gather corrected from the NMO, is shown in Fig. 9(a). The filtered seismograms, using the first and second 2D time-derivative, are shown in Figs 9(b) and 9(c), respectively. Figure 9(b) was used as input data to compute the second derivative. In addition to the attenuation of the ground-roll and the enhancement of the underlying reflections, a reduction of NMO stretch can be seen.

Figure 10 shows the original and the filtered common-shot gathers after applying the reverse NMO correction. The original seismograms are shown in Fig. 10(a) and the results obtained using the first and second 2D time-derivatives are shown in Figs 10(b) and 10(c), respectively. The ground-roll was practically removed, thus improving the signal-to-noise ratio and the lateral continuity of the reflection, formerly masked by noise.

Figure 11 shows the amplitude spectrum of the original and the filtered seismograms obtained using the FK and the time-derivative methods. When comparing the curves of Fig. 11, one notices that the new 2D time-derivative filtering approach produces attenuation of the amplitude spectrum in the frequency band of the ground-roll and an increase of the high frequency signal. This is not seen in the amplitude spectrum after FK filtering, which produces a severe cut in the low frequency band of the ground-roll.

As a consequence of the computational manipulation of the original seismograms (direct NMO, 2D time-derivative and reverse NMO) the waveform was affected and an additional filtering step can be applied to recover the original wavelet. This transformation may be performed by using the conventional least-squares shaping filter following the steps: (i) estimate the autocorrelation coefficients associated with the bandwidth frequency of the wavelet 15–50 Hz, of the

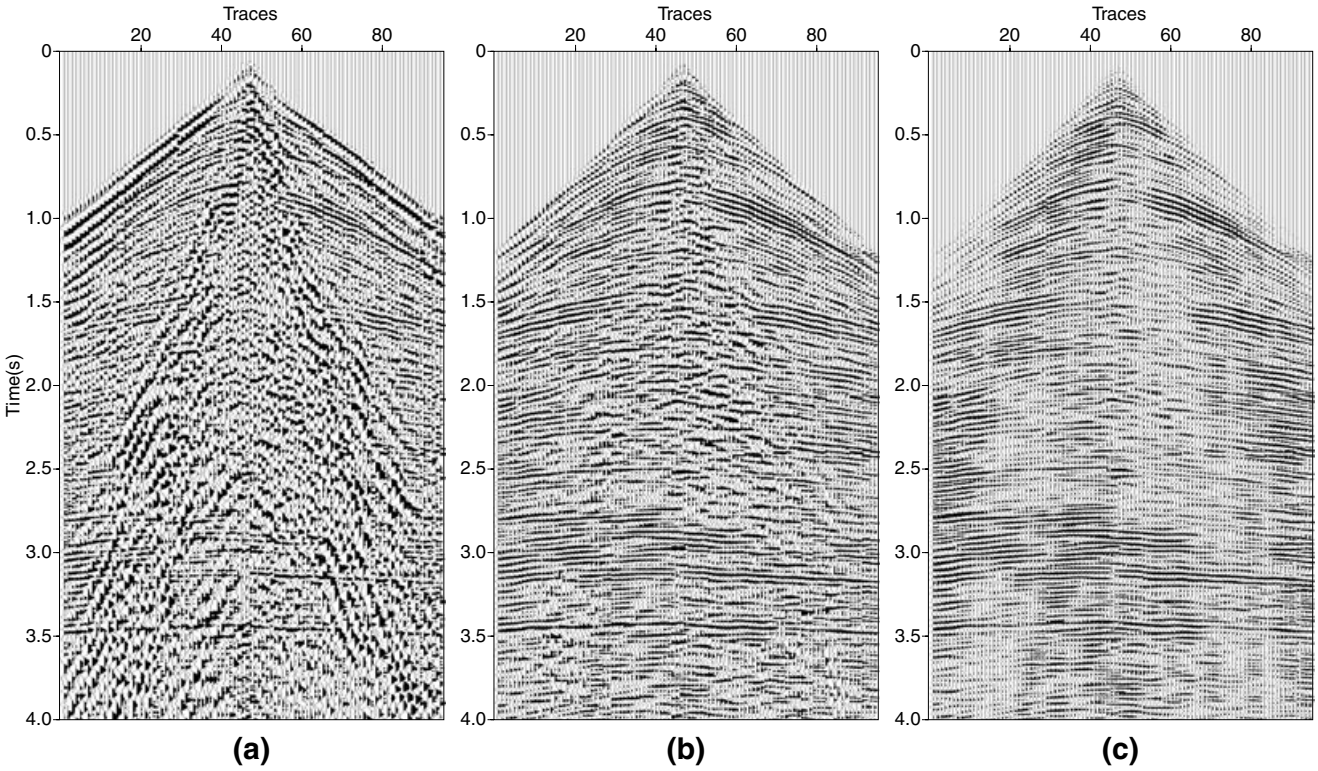

Figure 10 Reverse NMO correction of shot-gathers presented in Fig. 9. The first and second 2D time-derivatives are shown in (b) and (c), respectively.

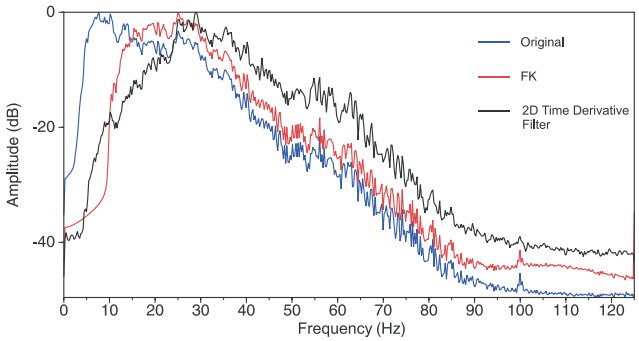

Figure 11 Amplitude spectra of the seismograms shown in Figs 9(a), 8(b) and 9(c).

input (Fig. 10a) and output seismograms (Fig. 10c); (ii) compute the minimum-phase wavelets associated with the original and the filtered seismograms; (iii) compute the shaping filter to recover the minimum-phase wavelet of the input seismograms and (iv) convolve the shaping filter with the filtered seismograms (Robinson and Treitel 1980; Porsani 1996).

Figure 12 shows the super-gather presented in Fig. 5 after applying the 2D filtering method and its corresponding velocity analysis. A better definition of the velocities in the semblance plot may be observed. Results as good as this could probably be obtained by using the low-cut plus mix and the FK filtering approaches.

Figures 13 and 14 show respectively the stacked seismic section after ground-roll attenuation using the FK method and the new approach. A mute was not applied to the data before the stacking. The same velocity function was used for the CMP stacking. The improvement in the definition of the reflectors is visible throughout the whole section. Better resolution and better lateral continuity can be seen in Fig. 14.

CONCLUSIONS

We present a new filtering method for the attenuation of ground-roll. The new method is based on the 2D time-derivative of the seismograms applied after NMO correction. The NMO correction makes the reflections approximately horizontal, thus generating ideal conditions for 2D or multichannel filters, which take advantage of the lateral coherence between the reflections. As the ground-roll is not flattened by the NMO correction, its contribution will be reduced after the 2D filtering process. The main problem with the NMO correction is the difficulty of making the initial velocity analysis in the presence of the ground-roll.

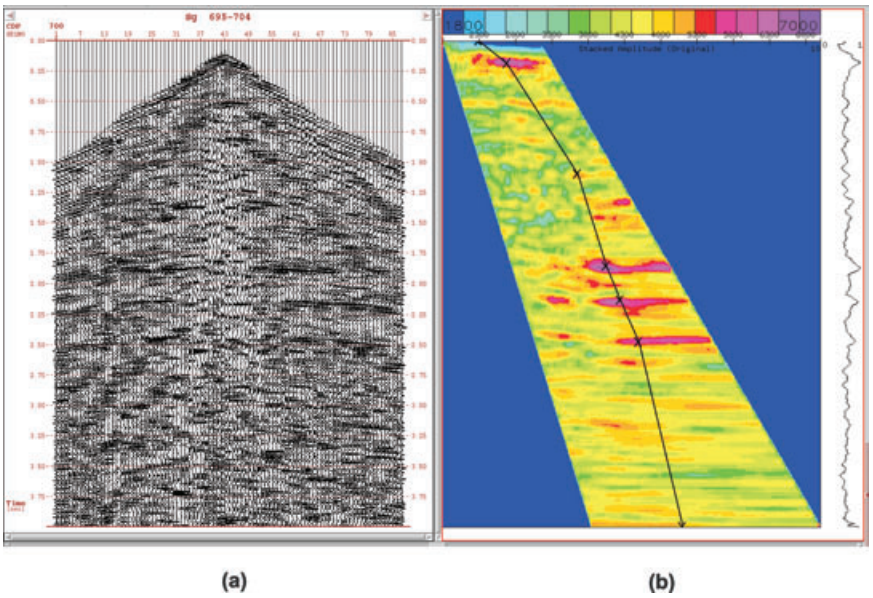

Figure 12 Super-gather shown in Fig. 5 filtered using the 2D derivative approach is shown in (a) and its corresponding velocity analysis in (b).

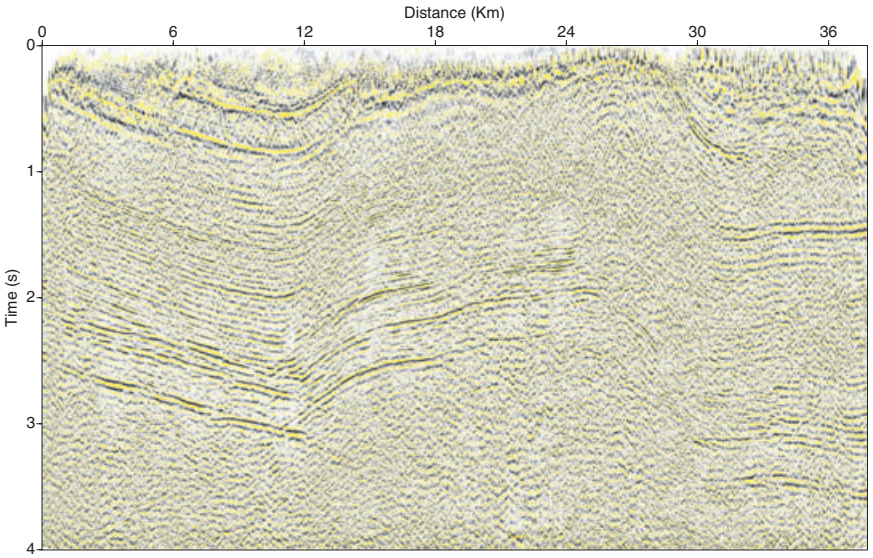

Figure 13. Stacked seismic line RL-5090 after ground-roll attenuation using the FK method.

The 2D filter coefficients are calculated once and the filter is applied to the whole data set by means of convolution, making the method computationally very efficient. Numerical results using real data demonstrate its effectiveness for the attenuation of the ground-roll. Additionally, the 2D time-derivative filtering method also attenuates NMO stretch, increases the signal-to-noise ratio and improves resolution. The attenuation of the ground-roll and the recovery of the underlying reflections can lead to improved velocity analysis on filtered CMPs. The final stacked section has higher resolution and lateral continuity, compared to the results obtained using the conventional FK method. New applications and extensions of the method for 2D or multi-dimensional directional filtering, using pre or post-stacking data, can be implemented.

ACKNOWLEDGEMENTS

The authors wish to express their gratitude to the Editor-in-Chief Dr Tijmen Jan Moser and the Associate Editor Dr John Sunderland as well as the anonymous referees for constructive

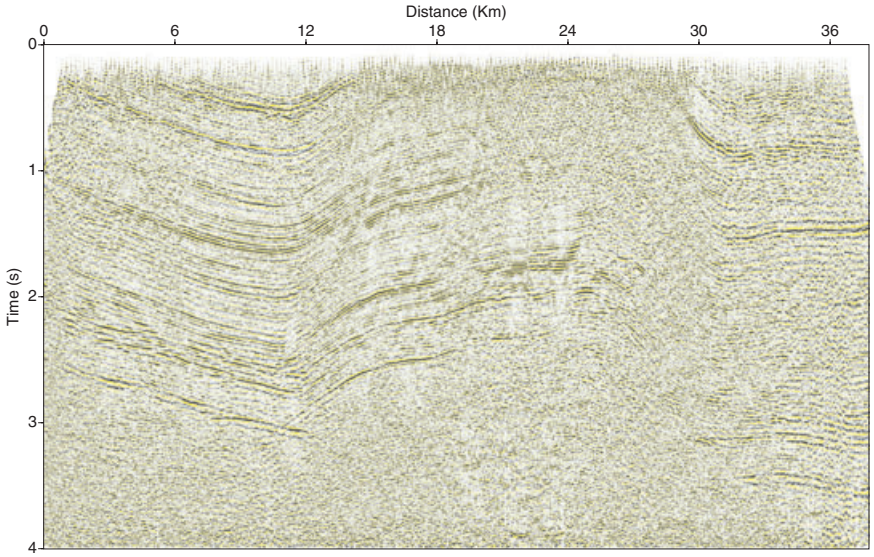

Figure 14. Stacked seismic line RL-5090 after ground-roll attenuation using the 2D time-derivative filtering method.

comments. We also thank FINEP, FAPESB, PETROBRAS, ANP and CNPq, Brazil for financial support and Paradigm, Landmark and Seismic-micro Technology for educational licenses granted to the Centro de Pesquisa em Geofísica e Geologia (CPGG-UFBA).

REFERENCES

Anstey N. 1986. Whatever happened to ground-roll? *The Leading Edge* **5**, 40–46.

Claerbout J.F. 1983. Ground Roll and radial traces. Stanford Exploration Project Report, SEP-35, 43–53.

Eiras J.F. and Kinoshita E.M. 1990. Geologia e perspectivas petrolíferas da Bacia do Tacutu, Origem e Evolução das Bacias Sedimentares. PETROBRAS, Anais, 197–220.

Embree P., Burg J.P. and Backus M.M. 1963. Wide-band velocity filtering - the pie-slice process. *Geophysics* **28**, 948–974.

Harlan W.S., Claerbout J.F. and Rocca F. 1984. Signal noise separation and velocity estimation. *Geophysics* **49**, 1869–1880.

Henley D.C. 2003. Coherent noise attenuation in the radial trace domain. *Geophysics* **68**, 1408–1416.

Kendall R., Jin S. and Ronen S. 2005. An SVD-polarization filter for ground roll attenuation on multicomponent data. 75th SEG meeting, Houston, Texas, USA, Expanded Abstracts, 928–931.

Liu X. 1999. Ground roll suppression using the Karhunen-Loeve transform. *Geophysics* **64**, 564.

Porsani M. 1996. Fast algorithms to design discrete Wiener filters in lag and length coordinates. *Geophysics* **61**, 882–890.

Pritchett W. 1991. System design for better seismic data. *The Leading Edge* **11**, 30–35.

Robinson E.A. and Treitel S. 1980. *Geophysical Signal Analysis*. Prentice-Hall.

Saatçilar R. and Canitez N. 1988. A method of ground-roll elimination. *Geophysics* **53**, 894.

Shepard D. 1968. A two-dimensional interpolation function for irregularly spaced data. Proceedings of the 23rd National Conference ACM, pp. 517–523. Brandon/Systems Press Inc., Princeton.

Shieh C. and Herrmann R.B. 1990. Ground roll: Rejection using polarization filters. *Geophysics* **55**, 1216. doi:10.1190/1.1442937

Song Y. and Stewart R.R. 1993. Ground roll rejection via f-v filtering. *CREWES Research Report* **5**.

Wiggins R.A. 1966. W-K Filter design. *Geophysical Prospecting* **14**, 427–440.

Yarham C., Boeniger U. and Herrmann F. 2006. Curvelet-based ground roll removal. 76th SEG meeting, New Orleans, Louisiana, USA, Expanded Abstracts, 2777–2780.

Yilmaz Ö. 1987. *Seismic Data Processing*. SEG.